



Synthetic electric fields and phonon damping in carbon nanotubes and graphene

Felix von Oppen,¹ Francisco Guinea,² and Eros Mariani¹

¹*Institut für Theoretische Physik, Freie Universität Berlin, Arnimallee 14, 14195 Berlin, Germany*

²*Instituto de Ciencia de Materiales de Madrid, CSIC, Cantoblanco, E28049 Madrid, Spain*

(Received 12 May 2009; published 18 August 2009)

Within the Dirac theory of the electronic properties of graphene, smoothly varying lattice strain affects the Dirac carriers through a synthetic gauge field. For static lattice strain, the gauge field induces a synthetic magnetic field which is known to suppress weak localization corrections by a dynamical breaking of time-reversal symmetry. When the lattice strain is time dependent, as in connection with phononic excitations, the gauge field becomes time dependent and the synthetic vector potential is also associated with an electric field. In this paper, we show that this synthetic electric field has observable consequences. We find that the Joule heating associated with the currents driven by the synthetic electric field dominates the intrinsic damping, caused by the electron-phonon interaction, of many acoustic phonon modes of graphene and metallic carbon nanotubes when including the effects of disorder and Coulomb interactions. Several important consequences follow from the observation that by time-reversal symmetry, the synthetic electric field associated with the vector potential has opposite signs for the two valleys. First, this implies that the synthetic electric field drives charge-neutral valley currents and is therefore unaffected by screening. This frequently makes the effects of the synthetic vector potential more relevant than a competing effect of the scalar deformation potential which has a much larger bare coupling constant. Second, valley currents decay by electron-electron scattering (valley Coulomb drag) which causes interesting temperature dependence of the damping rates. While our theory pertains first and foremost to metallic systems such as doped graphene and metallic carbon nanotubes, the underlying mechanisms should also be relevant for semiconducting carbon nanotubes when they are doped.

DOI: [10.1103/PhysRevB.80.075420](https://doi.org/10.1103/PhysRevB.80.075420)

PACS number(s): 62.25.-g, 63.20.kd, 63.22.Gh, 63.22.Np

I. INTRODUCTION

It is one of the remarkable aspects of the Dirac description of the low-energy electronic properties of graphene^{1,2} that both disorder and lattice strain give rise to synthetic gauge fields.³⁻⁷ If the synthetic vector potential $\mathbf{A}(\mathbf{r})$ is due to static disorder or static lattice distortions, its presence affects the electronic dynamics through an effective magnetic field $e\mathbf{B} = \nabla \times \mathbf{A}$ which, by time-reversal symmetry, points in opposite directions at the two Dirac points of the electronic dispersion. Consequences of this effective magnetic field have been widely studied in the literature.^{6,8-11} Additional physics arises when the synthetic vector potential is caused by *time-dependent* distortions such as phonons. In this case, \mathbf{A} becomes time dependent and will generate not only a magnetic but also an effective electric field $e\mathbf{E} = -\partial\mathbf{A}/\partial t$.

In this paper, we show that these synthetic electric fields have observable consequences. Consider a low-energy phonon mode of graphene or carbon nanotubes (CNT). The phonon is associated with a synthetic electric field which, when the system is metallic, drives currents. The dissipation (Joule heating) associated with these currents causes damping of the phonon mode. We find that frequently, the synthetic electric fields are directly responsible for the damping of phonon modes in metallic carbon nanotubes and graphene. In the clean limit, this damping mechanism is equivalent to dissipation by electron-hole pair creation. In fact, we find that we reproduce corresponding recent results for the radial breathing mode of clean carbon nanotubes.¹² Approaching the problem from the point of view of the synthetic electric fields allows us to calculate damping rates including the effects of disorder and electron-electron interactions which we

find to be significant. Moreover, we find appreciable damping rates even for those phonon modes of carbon nanotubes for which damping by electron-hole pair creation is not effective due to the large discrepancy between the electron and the phonon velocities. As a result, we expect damping by the electron-phonon interaction to dominate over other mechanisms such as phonon-phonon coupling¹³ over a wide range of parameters.

Searching for observable consequences of the synthetic electric field is complicated by the fact that lattice distortions do not only induce a vector potential \mathbf{A} but also a scalar potential⁵ $\phi(\mathbf{r}, t)$ which leads to an additional electric field $-\nabla\phi$. Within a tight-binding approach, the synthetic vector potential is associated with changes in the hopping amplitude caused by changes in the bond length. The scalar potential is a deformation potential which arises from local dilation or compression of the lattice. In fact, estimates⁵ suggest that the bare coupling constant of the scalar potential is about an order of magnitude larger than that of the vector potential.

Nevertheless, we find that the damping of most (but not all) low-energy phonon modes of graphene and carbon nanotubes is dominated by the vector potential. This is a consequence of two important qualitative differences between the electric fields associated with the scalar and vector potentials: (i) while the scalar field affects both valleys in the same manner, the sign of the vector potential is opposite for the two valleys. As a result, the currents driven by the electric fields are charge currents for the scalar potential, but valley currents for the vector potential. Therefore, the valley electric fields due to the vector potential will not be subject to screening as they do not induce any charge densities. Since in contrast, the electric fields arising from the scalar defor-

mation potential are screened, this may significantly affect the relative importance of the two electric fields when the system is metallic. (ii) The scalar potential is necessarily associated with a longitudinal electric field whose direction is parallel to the wave vector. In contrast, the vector potential generates a synthetic electric field which in general has both longitudinal and transverse components. We find that over a wide range of wave vectors, the transverse conductivity (and hence the corresponding dissipation) is significantly larger than the longitudinal conductivity.

The fact that the vector potential drives valley currents has another important consequence. While by momentum conservation, electron-electron interactions cannot induce a decay of charge currents, they do lead to a decay of valley currents by a process which is analogous to spin Coulomb drag.^{14–16} We find that this valley Coulomb drag mechanism leads to interesting temperature dependence of the phonon damping which in many cases is decreasing as temperature increases.

The damping mechanisms which we discuss apply most directly to systems with metallic behavior, i.e., metallic carbon nanotubes and graphene. For this reason, we will not explicitly discuss semiconducting CNT in this paper. It has recently been suggested¹³ that the intrinsic vibrational damping in semiconducting CNT is dominated by nonlinear elastic effects. However, it should be kept in mind that in practice, many semiconducting CNT are doped and can hence exhibit a finite conductivity. In this case, the damping mechanisms discussed in this paper may well be relevant as well.

It is found experimentally that the vibrational relaxation time of the radial breathing mode is remarkably long, of the order of several nanoseconds.¹⁷ This follows from scanning-tunneling-microscope-based transport measurements, in which the tunneling current excites the radial breathing mode, which enables vibron-absorption processes at temperatures far below the phonon frequency. We find that our results for the vibrational relaxation time of the radial breathing mode are consistent with these experiments.

Identifying parameters for which long vibrational relaxation times can be realized in CNT is also of much interest from the perspective of nanoelectromechanical systems made of carbon nanotubes^{12,17–22} and graphene.^{23–25} For example, if vibrational relaxation times are sufficiently long, these systems provide access to a regime in which the transport current drives the vibrational mode far out of thermal equilibrium. For strong electron-vibron coupling, this non-equilibrium regime can be characterized by self-similar avalanche transport.^{26,27} One of the most promising systems to observe this effect are suspended carbon nanotube quantum dots for which strong electron-vibron coupling and the associated Franck-Condon blockade have recently been confirmed experimentally.²²

This paper is organized as follows. In Sec. II, we introduce the strain-induced scalar and vector potentials (Sec. II A) and derive a general expression for the relation between the phonon damping rate and the conductivity (Sec. II B). We also illustrate the basic physical picture in the context of the radial breathing modes of carbon nanotubes (Sec. II C). Our approach allows us to include the effects of disorder (Sec. III) and of electron-electron interactions (Sec. IV) on

phonon damping. Finally we conclude in Sec. V. Some calculational details are relegated to the Appendix.

II. BASIC FORMALISM

A. Strain-induced vector and scalar potentials

Elastic strains couple to electrons in graphene and carbon nanotubes by inducing effective scalar and vector potentials into the low-energy electronic Dirac Hamiltonian,³

$$\mathcal{H} = \int d^2\mathbf{r} \Psi^\dagger(\mathbf{r}) \{v_F [i\sigma_i(\partial_i - A_i)] + \phi\} \Psi(\mathbf{r}), \quad (1)$$

where $\Psi(\mathbf{r})$ is the spinor which defines the electron, σ_i is a Pauli matrix, v_F is the Fermi velocity, and we show the Hamiltonian defined for one of the two, K and K' , valleys in the Brillouin zone of graphene. Here we chose coordinates such that the unit vectors of the graphene lattice can be written as

$$\begin{aligned} \mathbf{a}_1 &= a\sqrt{3} \left(\frac{\sqrt{3}}{2} \mathbf{n}_x + \frac{1}{2} \mathbf{n}_y \right), \\ \mathbf{a}_2 &= a\sqrt{3} \left(\frac{\sqrt{3}}{2} \mathbf{n}_x - \frac{1}{2} \mathbf{n}_y \right), \end{aligned} \quad (2)$$

where $a \approx 1.4 \text{ \AA}$ denotes the bond length. Both the vector and the scalar potential can be expressed in terms of the strain tensor u_{ij} . The scalar potential is determined by the trace of the strain tensor, $\phi(\mathbf{r}, t) = g_D(u_{xx} + u_{yy})$, where g_D is estimated to be of order 20–30 eV in Ref. 5. The form of the vector potential is essentially fixed by symmetry to be^{7,10}

$$\mathbf{A}(\mathbf{r}) = \frac{\hbar\beta}{2a} \begin{pmatrix} 2u_{xy} \\ u_{xx} - u_{yy} \end{pmatrix}, \quad (3)$$

where $\beta = \partial \log(t) / \partial \log(a) \approx 2-3$. Strictly speaking, this expression has a small uncertainty in the prefactor since the theory of elasticity may not accurately describe the displacements within the unit cell.

In nanotubes, the natural coordinate system, defined by the nanotube axis, is rotated by an angle θ with respect to the coordinate axes of graphene defined above. Choosing the CNT axis as the x axis and the direction around the tube as the y axis, the angle θ is given by $\cot \theta = \sqrt{3} \frac{n-m}{n+m}$ for (n, m) carbon nanotubes. It takes the value $\theta=0$ ($\theta=\pi/2$) for zigzag (armchair) CNT. The vector potential takes the form

$$\mathbf{A}(\mathbf{r}) = \frac{\hbar\beta}{2a} D(3\theta) \begin{pmatrix} 2u_{xy} \\ u_{xx} - u_{yy} \end{pmatrix}, \quad (4)$$

where $D(3\theta)$ is a rotation matrix. Note that in this equation, also the strain tensor is given in the rotated coordinate system.

The acoustic phonon modes of carbon nanotubes and graphene can be described within standard elasticity theory. For graphene, the elastic Lagrangian density for the strain tensor u_{ij} and the out-of-plane displacement $h(\mathbf{r}, t)$ takes the form

$$\mathcal{L} = T - V_{\text{stretch}} - V_{\text{bend}} \quad (5)$$

with

$$\begin{aligned} T &= \frac{\rho_0}{2} (\dot{\mathbf{u}}^2 + \dot{h}^2), \\ V_{\text{stretch}} &= \mu u_{ij}^2 + \frac{1}{2} \lambda u_{kk}^2, \\ V_{\text{bend}} &= \frac{1}{2} \kappa (\nabla^2 h)^2 \end{aligned} \quad (6)$$

in terms of the two-dimensional (2D) mass density ρ_0 , the Lamé coefficients μ and λ characterizing the in-plane rigidity of the lattice, and the bending rigidity κ . The same Lagrangian also applies to carbon nanotubes of radius R , when replacing the bending energy by

$$V_{\text{bend}} = \frac{1}{2} \kappa \left(\nabla^2 h + \frac{h}{R^2} \right)^2. \quad (7)$$

The strain tensor takes the form $u_{ij} = (1/2)[\partial_i u_j + \partial_j u_i + (\partial_i h)(\partial_j h)]$ for graphene and

$$\begin{aligned} u_{xx} &= \frac{\partial u_x}{\partial x}, \\ u_{yy} &= \frac{\partial u_y}{\partial y} + \frac{h}{R}, \\ u_{xy} &= \frac{1}{2} \left(\frac{\partial u_y}{\partial x} + \frac{\partial u_x}{\partial y} \right), \end{aligned} \quad (8)$$

for carbon nanotubes. Here, \mathbf{u} denotes the displacements within the graphene sheet and h the displacement in the perpendicular (for CNT: radial) direction.

B. Phonon damping

As argued in the Introduction, there is a close relation between phonon damping and the conductivity tensor. This relation can be obtained formally by computing the shift $\Delta\omega$ in the phonon frequency due the electron-phonon coupling. The damping rate is then given by $\Gamma = 2 \text{Im} \Delta\omega$. Consider first the case in which the phonon is associated with a vector potential $\mathbf{A}(\mathbf{r}, t)$. We can express the vector potential in terms of phonon creation and annihilation operators, $b_{\mathbf{q}}$ and $b_{\mathbf{q}}^\dagger$, respectively,

$$\begin{aligned} \mathbf{A}(\mathbf{r}, t) &= \frac{1}{2\Omega} \sum_{\mathbf{q}} \mathcal{A}_{\mathbf{q}} \exp(i\mathbf{q}\mathbf{r}) \\ &\times [b_{\mathbf{q}} \exp(-i\omega_{\mathbf{q}}t) + b_{-\mathbf{q}}^\dagger \exp(i\omega_{\mathbf{q}}t)] \end{aligned} \quad (9)$$

with

$$\mathcal{A}_{\mathbf{q}} = \frac{\hbar\beta}{2a} \sqrt{\frac{2\hbar\Omega}{\rho_0\omega_{\mathbf{q}}}} [D(3\theta)M_{\mathbf{q}}\hat{\mathbf{p}}]. \quad (10)$$

Here, we defined the matrix

$$M_{\mathbf{q}} = \begin{pmatrix} iq_y & iq_x & 0 \\ iq_x & -iq_y & -1/R \end{pmatrix} \quad (11)$$

and a unit vector $\hat{\mathbf{p}}$ describing the mode polarization in u_x , u_y , and h direction, which takes the form $\hat{\mathbf{p}} = [1, 0, i\lambda q_x R / (2\mu + \lambda)]$ for the longitudinal stretching mode, $\hat{\mathbf{p}} = (0, 1, 0)$ for the twist mode, and $\hat{\mathbf{p}} = (0, 0, 1)$ for the radial breathing mode [as obtained from the Euler-Lagrange equations for the elastic Lagrangian Eq. (5)]. The surface area of the nanotube is denoted by $\Omega = (2\pi R)L$ and the mode dispersion by $\omega_{\mathbf{q}}$. The corresponding results for the acoustic modes of graphene follow by taking $R \rightarrow \infty$ and setting $\theta = 0$. (The flexural modes of graphene will be discussed separately below.)

In second-order perturbation theory, we then find for the damping rate of a phonon with wave-vector \mathbf{q} ,

$$\begin{aligned} \Gamma_{\mathbf{q}} &= \frac{\pi}{2\hbar\Omega^2} \sum_{\epsilon_\beta > E_F} \sum_{\epsilon_\alpha < E_F} |\langle \beta | v_F \sigma \cdot \mathcal{A}_{\mathbf{q}} \exp(i\mathbf{q}\mathbf{r}) | \alpha \rangle|^2 \\ &\times \delta(\epsilon_\beta - \epsilon_\alpha - \hbar\omega_{\mathbf{q}}). \end{aligned} \quad (12)$$

Using the Kubo formula, we can express $\Gamma_{\mathbf{q}}$ in terms of the dissipative (real and symmetric) contribution $\sigma_s(\mathbf{q}, \omega)$ to the conductivity tensor,

$$\begin{aligned} \sigma_{s;kl}(\mathbf{q}, \omega) &= \frac{\pi e^2}{\Omega\omega} \text{Re} \sum_{\epsilon_\beta > E_F} \sum_{\epsilon_\alpha < E_F} \langle \beta | v_k \exp(i\mathbf{q}\mathbf{r}) | \alpha \rangle \\ &\times \langle \alpha | v_l \exp(-i\mathbf{q}\mathbf{r}) | \beta \rangle \delta(\epsilon_\beta - \epsilon_\alpha - \hbar\omega). \end{aligned} \quad (13)$$

Here, $\mathbf{v} = v_F \sigma$ denotes the velocity operator. Note that we employ the two-dimensional conductivity unless explicitly stated otherwise. Thus, we can express the damping rate as

$$\Gamma_{\mathbf{q}} = \frac{\omega_{\mathbf{q}}}{2e^2\hbar\Omega} \sigma_{s;ij}(\mathbf{q}, \omega) \left(\mathcal{A}_{\mathbf{q};i}^* + \frac{q_i}{\omega_{\mathbf{q}}} \phi_{\mathbf{q}}^* \right) \left(\mathcal{A}_{\mathbf{q};j} + \frac{q_j}{\omega_{\mathbf{q}}} \phi_{\mathbf{q}} \right). \quad (14)$$

Here, we have also included the effect of the scalar potential ϕ and defined³¹

$$\phi_{\mathbf{q}} = \frac{g_D}{1 + v(\mathbf{q})\Pi(\mathbf{q}, \omega)} \sqrt{\frac{2\hbar\Omega}{\rho_0\omega_{\mathbf{q}}}} \mathbf{M}_{\mathbf{q}}^\phi \cdot \hat{\mathbf{p}} \quad (15)$$

in terms of the vector

$$\mathbf{M}_{\mathbf{q}}^\phi = (iq_x, iq_y, 1/R). \quad (16)$$

Note that we have included the effects of screening in the contribution originating from the scalar potential. [$v(\mathbf{q})$ denotes the Coulomb interaction and $\Pi(\mathbf{q}, \omega)$ the polarization operator].

In the remainder of the paper, we discuss the dynamic conductivity $\sigma(\mathbf{q}, \omega)$ within a quasiclassical approximation. This is justified for doped graphene when $k_F \max\{\ell, 1/q\} \gg 1$ where ℓ denotes the elastic mean-free path.

C. Basic physical picture: Damping of the radial breathing mode in armchair CNT

Before we embark on a systematic investigation of phonon damping based on the expressions derived above, we would like to illustrate the basic physics in the context of the radial breathing mode of armchair carbon nanotubes. We will do this in the context of a semiclassical approach which clearly brings out the physics and complements the more quantum-mechanical approach taken in the remainder of the paper. This example also shows that our approach yields damping rates which are of the order of those observed in experiment.¹⁷

For the radial breathing mode (RBM) of carbon nanotubes, only the radial displacement h is nonzero (i.e., $\mathbf{u}=0$) in the long-wavelength limit. According to Eq. (8), the corresponding strain tensor takes the form $u_{xx}=u_{xy}=0$ while $u_{yy}=h/R$. Using that for armchair carbon nanotubes $\theta=\pi/2$, the synthetic vector potential takes the form

$$\mathbf{A}(\mathbf{r},t) = \frac{\hbar\beta}{2a} \begin{pmatrix} h(\mathbf{r},t)/R \\ 0 \end{pmatrix}. \quad (17)$$

Similarly, we find for the scalar deformation-potential $\phi(\mathbf{r},t)=g_D h(\mathbf{r},t)/R$. In the long-wavelength limit $q \rightarrow 0$, the electric field $-\nabla\phi$ associated with the scalar potential vanishes. At the same time, the valley electric field $e\mathbf{E}=-\partial\mathbf{A}/\partial t$ originating from the vector potential remains finite because the RBM dispersion tends to a finite frequency $\omega_B=[(2\mu+\lambda)/\rho_0 R^2]^{1/2}$ for $q \rightarrow 0$. Thus, the synthetic vector potential gives the dominant contribution to the damping of the radial breathing mode. Note also that the electric field is pointing in the direction along the nanotube axis.

For clean armchair carbon nanotubes, the damping of the radial breathing mode vanishes to leading order,¹² since the contribution of the synthetic vector potential to the Hamiltonian is proportional to σ_x and hence commutes with the unperturbed Hamiltonian. However, since armchair carbon nanotubes are metallic, there will be damping in the presence of disorder. Describing the optical conductivity of carbon nanotubes within a Drude model, we have

$$\sigma(\omega) = \frac{\sigma_{dc}}{1 - i\omega\tau} \quad (18)$$

in terms of the mean-free time τ . From the Einstein relation, the [one-dimensional (1D)] dc conductivity takes the form $\sigma_{dc} = \frac{Ne^2}{\pi\hbar} \ell$, where $\ell = v_F \tau$ denotes the electronic mean-free path and N counts the spin and valley degeneracy. We can now compute the damping rate of the radial breathing mode, Γ , by equating the time derivative of the elastic energy \mathcal{E} with the Joule heating associated with $\text{Re } \sigma(\omega)$.

The elastic energy of the radial breathing mode (per unit length) can be readily obtained from the elastic Lagrangian so that we find

$$\frac{d\mathcal{E}}{dt} = \frac{d}{dt} [(2\pi R)\rho_0\omega_B^2 |h(\omega_B)|^2] = -\text{Re } \sigma(\omega_B) |\mathbf{E}(\omega_B)|^2 = \hbar\omega_B\Gamma. \quad (19)$$

Inserting $e|\mathbf{E}(\omega)| = \frac{\hbar\beta\omega_B}{2aR} |h(\omega)|$ for the synthetic electric field, we find a damping rate Γ of

$$\Gamma = \frac{N\hbar\beta^2}{8\pi^2(\rho_0 a^2)R^3} \frac{\ell}{1 + (\omega_B\tau)^2}. \quad (20)$$

An interesting aspect of this expression is that the damping rate falls off with the third power of the nanotube radius. This may be useful guidance to enter into the regime of current-driven nonequilibrium in nanoelectromechanical devices.

Numerical estimates of Eq. (20) yield relaxation times on the order of nanoseconds for an elastic mean-free path of 1 μm and a diameter of order 1 nm. This is of the same magnitude as the relaxation times observed in experiment.¹⁷

III. DISORDER EFFECTS ON PHONON DAMPING

A. Carbon nanotubes

Due to the weakness of screening in one dimension, the scalar potential remains relevant in carbon nanotubes. Indeed, one readily estimates that in the absence of screening, the ratio of the electric fields due to vector and scalar potential is of the order

$$\frac{E_A}{E_\phi} \sim \frac{\omega A}{q\phi} \sim \frac{\hbar c\beta}{ag_D} \sim 10^{-2} \quad (21)$$

for phonon modes with a linear dispersion $\omega=cq$. At the same time, the suppression of the scalar potential by screening

$$[1 + v(\mathbf{q})\Pi(\mathbf{q},\omega)]^{-1} \simeq \left[1 + \frac{e^2\nu}{\pi} \ln(1/qR) \right]^{-1} \quad (22)$$

involves, for realistic values of q , a factor smaller than but still of order one. Here, ν denotes the electronic density of states and R the radius of the nanotube. As a result, we conclude that the damping of the longitudinal stretching mode is dominated by the effects of the scalar potential. In contrast, the damping of the radial breathing mode (whose dispersion approaches a finite frequency as $q \rightarrow 0$) will be dominated by the vector potential. In the following, we will only discuss the dominant dissipation channel for the various phonon modes of carbon nanotubes. An evaluation of the subdominant dissipation channel would, however, be straightforward.

1. Radial breathing mode

In order to make contact with the literature,¹⁷ it is instructive to start with the damping of the radial breathing mode in clean carbon nanotubes. One readily establishes that only the y component of the vector potential

$$A_{\mathbf{q}} = -\frac{\hbar\beta}{2aR} \sqrt{\frac{2\hbar\Omega}{\rho_0\omega_{\mathbf{q}}}} \begin{pmatrix} -\sin(3\theta) \\ \cos(3\theta) \end{pmatrix} \quad (23)$$

contributes to dissipation. Evaluating Eq. (13), we obtain for the corresponding component of the dissipative conductivity tensor

$$\sigma_{yy}(\omega) = \frac{Ne^2v_F}{2\hbar R\omega} \theta(\omega - 2v_Fk_F). \quad (24)$$

Inserting Eqs. (23) and (24) into the general expression Eq. (14), we recover for the damping rate of the RBM of clean carbon nanotubes¹⁷

$$\Gamma_{\text{RBM}} = \frac{N\hbar\beta^2v_F}{8(\rho_0a^2)R^3\omega} \cos^2(3\theta) \theta(\omega - 2v_Fk_F). \quad (25)$$

Specifically, this expression confirms the absence of damping for armchair CNT where $\theta = \pi/2$. This shows that our approach is equivalent to standard approaches to damping of phonon modes.

The strength of making the relation with the synthetic electric fields lies in allowing us to go beyond the limit of clean and noninteracting samples. Including disorder for the armchair CNT, there will also be damping due to electric fields pointing along the CNT. Again using a Drude expression for the frequency-dependent conductivity, one recovers from Eq. (14) the semiclassical result given above in Eq. (20).

2. Longitudinal stretching mode

At long wavelengths, the longitudinal stretching mode of carbon nanotubes has a much lower frequency $\omega = cq$ than the radial breathing mode and we can make a diffusive ansatz for the dynamic conductivity,

$$\sigma(\mathbf{q}, \omega) = \frac{-i\omega\sigma_{\text{dc}}}{-i\omega + Dq^2}, \quad (26)$$

which is valid when $q\ell \ll 1$ and $D = v_F\ell/2$ is the diffusion coefficient. Note that the diffusion pole in this expression is protected by charge conservation since the scalar potential drives ordinary charge currents. The dissipative conductivity is then given by

$$\text{Re } \sigma(\mathbf{q}, \omega) = \frac{\omega^2\sigma_{\text{dc}}}{\omega^2 + (Dq^2)^2}. \quad (27)$$

The precise q dependence of the conductivity depends sensitively on the relative magnitudes of $\omega = cq$ and Dq^2 . To clearly bring out the q dependence of the damping rate, we consider the long-wavelength regime $q \ll q_0$, dominated by ω , and the short-wavelength regime $q \gg q_0$, dominated by Dq^2 , separately. Here, the characteristic wave vector dividing between these two regimes is given by

$$q_0 = 2\frac{c}{v_F}\frac{1}{\ell}. \quad (28)$$

Evaluating the scalar potential Eq. (15) for the longitudinal stretching mode and inserting the resulting expression into Eq. (14), we obtain the damping rate

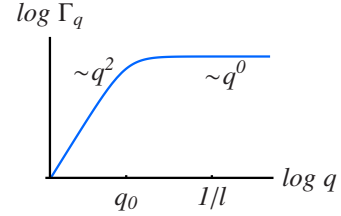


FIG. 1. (Color online) Sketch of the damping rate as function of wave vector for the longitudinal stretching mode of carbon nanotubes.

$$\Gamma_{\mathbf{q}} \simeq \frac{2Ng_D^{*2}}{\pi^2\hbar\rho_0Rv_F^2\ell} \begin{cases} (q/q_0)^2, & q \ll q_0 \\ 1, & q \gg q_0 \end{cases}. \quad (29)$$

Here, we defined the renormalized coupling-constant

$$g_D^* = \frac{g_D}{1 + \frac{Ne^2}{\pi^2\hbar v_F} \ln(1/qR)}, \quad (30)$$

which, strictly speaking, still includes a weak logarithmic q dependence.

Equation (29) predicts that the damping rate increases quadratically with q for long wavelengths and saturates to a \mathbf{q} -independent constant for shorter wavelengths $q \gg q_0$. This behavior is sketched in Fig. 1. It is interesting to compare $\Gamma_{\mathbf{q}}$ to the mode frequency $\omega_{\mathbf{q}}$ in order to see whether the longitudinal stretching mode can become overdamped for some region of wave vectors. Clearly, the ratio $\Gamma_{\mathbf{q}}/\omega_{\mathbf{q}}$ is maximal for $q = q_0$. Remarkably, the maximal value of this ratio becomes independent of the elastic mean-free path and thus quite universal,

$$\frac{\Gamma_{q_0}}{\omega_{q_0}} = \frac{Ng_D^{*2}}{\pi^2\rho_0R\hbar v_F c^2}. \quad (31)$$

Inserting numbers typical of carbon nanotubes into this expression, one finds values of order 0.1 showing that even though the longitudinal stretching mode remains underdamped at all wavelengths, damping can be quite significant.

B. Graphene

1. Longitudinal and transverse-acoustic (in-plane) phonons

The analysis of the previous section can be extended to phonon modes of graphene. However, phonon damping in (doped) graphene will typically be dominated by the vector potential. At long wavelengths, this is a consequence of the much stronger screening in two dimensions than in the carbon nanotube setting,

$$\frac{1}{1 + v(\mathbf{q})\Pi(\mathbf{q}, \omega)} \simeq \frac{q}{q + q_{\text{TF}}}, \quad (32)$$

where $q_{\text{TF}} = 2\pi e^2\nu$ denotes the Thomas-Fermi wave vector of graphene. (For a density of approximately 10^{12} cm^{-2} , the screening length is on the order of tens of nm.) At short phonon wavelengths (relative to the elastic mean-free path), this emerges from the fact that unlike $-\nabla\phi$, $\mathbf{E} = -\partial\mathbf{A}/\partial t$ will

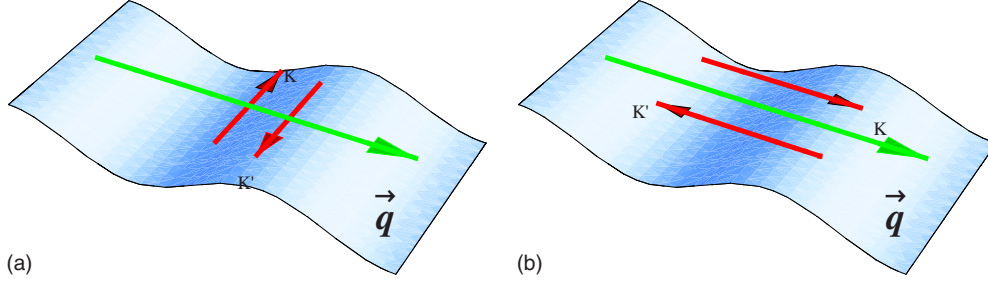


FIG. 2. (Color online) Orientation of the synthetic electric field at the two \mathbf{K} points of the dispersion (red arrows) with respect to the phonon wave-vector \mathbf{q} for (a) the purely transverse and (b) the purely longitudinal situation. As shown in Eqs. (33)–(36), the synthetic electric field is in general is neither purely parallel nor transverse.

almost always have a significant *transverse* component (relative to the wave-vector \mathbf{q} , cf. Figure 2).³² It turns out that in this range of wave vectors, the transverse conductivity (and hence the associated damping) is much larger than the longitudinal conductivity. In addition, even when the synthetic electric field is purely longitudinal, the weaker bare coupling of the vector potential is partially offset by the fact that dissipation by longitudinal valley currents is very sensitive to (and strongly enhanced by) disorder-induced intervalley scattering. (It is interesting to note that in the context of multi-valley semiconductors, the importance of intervalley scattering in acoustic attenuation is actually known for many decades).²⁸

Using Eq. (3), we can readily obtain the longitudinal and transverse components of the vector potential. Consistent with the lattice symmetry, we find

$$A_{\mathbf{q},\parallel} = \frac{\hbar\beta}{2a} \sqrt{\frac{2\hbar\Omega}{\rho_0\omega_{\mathbf{q}}}} iq \sin 3\theta_{\mathbf{q}}, \quad (33)$$

$$A_{\mathbf{q},\perp} = \frac{\hbar\beta}{2a} \sqrt{\frac{2\hbar\Omega}{\rho_0\omega_{\mathbf{q}}}} iq \cos 3\theta_{\mathbf{q}} \quad (34)$$

for the longitudinal phonon and

$$A_{\mathbf{q},\parallel} = \frac{\hbar\beta}{2a} \sqrt{\frac{2\hbar\Omega}{\rho_0\omega_{\mathbf{q}}}} iq \cos 3\theta_{\mathbf{q}}, \quad (35)$$

$$A_{\mathbf{q},\perp} = \frac{\hbar\beta}{2a} \sqrt{\frac{2\hbar\Omega}{\rho_0\omega_{\mathbf{q}}}} iq \sin 3\theta_{\mathbf{q}} \quad (36)$$

for the transverse phonons. Here, $\theta_{\mathbf{q}}$ denotes the angle between the direction of the wave-vector \mathbf{q} and the x axis.

At finite \mathbf{q} , the dissipative conductivity becomes a symmetric tensor which is diagonal in a coordinate system whose axes are parallel and perpendicular to the wave-vector \mathbf{q} ,

$$\sigma(\mathbf{q}, \omega) = \begin{pmatrix} \sigma_{\parallel}(\mathbf{q}, \omega) & 0 \\ 0 & \sigma_{\perp}(\mathbf{q}, \omega) \end{pmatrix}. \quad (37)$$

For doped graphene in the diffusive regime $q\ell \ll 1$, the longitudinal and transverse conductivities can be obtained from hydrodynamic equations for charge densities and currents which follow from a Boltzmann equation. One finds the continuity equations

$$\frac{\partial n_1}{\partial t} + \nabla \cdot \mathbf{j}_1 = -\frac{1}{\tau_V}(n_1 - n_2), \quad (38)$$

$$\frac{\partial n_2}{\partial t} + \nabla \cdot \mathbf{j}_2 = -\frac{1}{\tau_V}(n_2 - n_1), \quad (39)$$

as well as Ohm's laws

$$\left(\frac{1}{\tau} + \frac{1}{\tau_V}\right)\mathbf{j}_1 - \frac{1}{\tau_V}\mathbf{j}_2 = -\frac{v_F^2}{2}\nabla\rho_1 + \frac{e^2v_F^2}{2}\mathbf{E}_1, \quad (40)$$

$$-\frac{1}{\tau_V}\mathbf{j}_1 + \left(\frac{1}{\tau} + \frac{1}{\tau_V}\right)\mathbf{j}_2 = -\frac{v_F^2}{2}\nabla\rho_2 + \frac{e^2v_F^2}{2}\mathbf{E}_2. \quad (41)$$

Here, the indices 1 and 2 label the valleys, ν denotes the density of states, and $1/\tau$ and $1/\tau_V$ are the intravalley and intervalley scattering rates due to disorder, respectively. We left out the effects of induced electric fields from these equations because screening does not affect the valley odd channel. We can now obtain the valley-odd conductivity relating $\mathbf{E}_- = \mathbf{E}_1 - \mathbf{E}_2$ to $\mathbf{j}_- = \mathbf{j}_1 - \mathbf{j}_2$ by taking the difference between the two Eqs. (40) and (41), combined with the continuity equation in the valley-odd channel.

For the longitudinal conductivity, we find

$$\sigma_{\parallel}(\mathbf{q}, \omega) = \frac{\left(-i\omega + \frac{2}{\tau_V}\right)\sigma_{\text{dc}}}{-i\omega + Dq^2 + \frac{2}{\tau_V}}. \quad (42)$$

The reason for the cutoff of the diffusion pole by the intervalley scattering rate $1/\tau_V$ is that there is no conservation law associated with valley currents which is analogous to charge conservation for ordinary charge currents. Despite the weakness of intervalley scattering (originating from atomic-scale defects) compared to intravalley scattering, it is actually rather important to include $1/\tau_V$. From Eq. (42), the dissipative conductivity takes the form

$$\text{Re } \sigma_{\parallel}(\mathbf{q}, \omega) = \frac{\left[\omega^2 + \frac{2}{\tau_V}\left(Dq^2 + \frac{2}{\tau_V}\right)\right]\sigma_{\text{dc}}}{\omega^2 + \left(Dq^2 + \frac{2}{\tau_V}\right)^2}. \quad (43)$$

While it is evidently possible to work with this complete expression, it is more instructive to analyze the various limiting cases. Except for the scale $q_0 = (2c/v_F)(1/\ell)$ introduced above, this expression involves the intervalley scattering length $\ell_V = [\frac{1}{2}D\tau_V]^{1/2}$ as a second length scale. When $q\ell_V$

$\ll 1$, one finds that $\text{Re } \sigma_{\parallel}(\mathbf{q}, \omega) \approx \sigma_{\text{dc}}$. In the opposite limit $q\ell_V \gg 1$, one obtains

$$\text{Re } \sigma_{\parallel}(\mathbf{q}, \omega) \approx \begin{cases} \sigma_{\text{dc}}, & q \ll q_0 \\ \frac{1 + (q_0\ell_V)^2}{(q\ell_V)^2} \sigma_{\text{dc}}, & q \gg q_0 \end{cases}. \quad (44)$$

Transverse fields do not induce any charge densities and therefore, we find

$$\sigma_{\perp}(\mathbf{q}, \omega) = \sigma_{\text{dc}} \quad (45)$$

for the transverse conductivity at any $q \ll 1/\ell$.

For doped graphene in the ballistic regime $q\ell \gg 1$, we can obtain the dynamic conductivity $\sigma(\mathbf{q}, \omega)$ from the Boltzmann equation. Heuristically, we can obtain $\sigma(\mathbf{q}, \omega)$ (up to numerical prefactors) by making the replacements $Dq^2 \rightarrow v_F q$ and $1/\ell \rightarrow q$ in the diffusive results Eqs. (43) and (45). A more formal derivation is relegated to the Appendix. For transverse electric fields, disorder-induced intervalley scattering is irrelevant (since no valley charge densities are induced) so that the transverse conductivity becomes

$$\sigma_{\perp}(\mathbf{q}, \omega) = \frac{Ne^2 k_F}{h q} \quad (46)$$

for $\omega \ll v_F q$. It is interesting to note that this transverse conductivity σ_{\perp} also controls the attenuation of surface acoustic waves in the fractional quantum Hall effect at Landau-level filling factor $\nu = 1/2$.²⁹ In contrast, intervalley scattering is important for the longitudinal conductivity when $q_0\ell_V \ll 1$,

$$\sigma_{\parallel}(\mathbf{q}, \omega) = \begin{cases} \frac{e^2 \nu}{q^2 \tau_V}, & q \ll \frac{1}{(q_0\ell_V)^2 \ell} \\ \frac{e^2 \nu \omega^2}{v_F q^3}, & q \gg \frac{1}{(q_0\ell_V)^2 \ell} \end{cases}, \quad (47)$$

while for $q_0\ell_V \gg 1$, we find

$$\sigma_{\parallel}(\mathbf{q}, \omega) = \frac{e^2 \nu \omega^2}{v_F q^3} \quad (48)$$

for all $q \gg 1/\ell$. One readily establishes that $\sigma_{\parallel}/\sigma_{\perp} \sim (c/v_F)^2 \sim 10^{-4}$ for sufficiently large q , confirming that the damping will be dominated by the transverse conductivity except in a very narrow range of directions of \mathbf{q} where the synthetic electric field is almost purely longitudinal.

We are now in a position to combine these results with Eq. (14) and obtain the phonon damping rate in graphene over the full range of wave vectors. Whenever the synthetic electric field has an appreciable transverse component, we find

$$\Gamma_{\mathbf{q}} = \frac{N\hbar\beta^2 k_F}{8\pi\rho_0 a^2} f(\theta_{\mathbf{q}}) \begin{cases} q^2 \ell / 2, & q\ell \ll 1 \\ q, & q\ell \gg 1 \end{cases}. \quad (49)$$

Here, we defined the function $f(\theta)$ which is equal to unity deep in the diffusive regime, and crosses over to $f(\theta) = \cos^2 3\theta$ for transverse phonons and $f(\theta) = \sin^2 3\theta$ for longitudinal phonons.³³ Thus, we find that the phonon modes are underdamped at long-wavelengths $q\ell \ll 1$, but become marginal for $q\ell \gg 1$. Inserting numbers, we find that $\Gamma_{\mathbf{q}}$

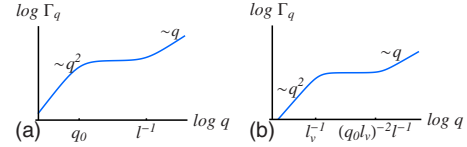


FIG. 3. (Color online) Schematic dependence of the damping rate $\Gamma_{\mathbf{q}}$ on wave-vector \mathbf{q} of acoustic phonons in graphene when the synthetic electric field is purely longitudinal, cf. Eqs. (50) and (51). This applies when the wave vector points in a narrow cone around the zigzag (armchair) direction for the longitudinal (transverse) acoustic phonon. Left: $q_0 > \ell_V^{-1}$. Right: $q_0 < \ell_V^{-1}$.

$\approx 10^{-2} \omega_{\mathbf{q}}$ in this marginal regime so that the phonon mode remains well-defined.

Whenever $f(\theta)$ is close to zero, the damping is dominated by the longitudinal conductivity. Specifically, this happens when \mathbf{q} points in the zigzag (armchair) direction for longitudinal (transverse) phonons. In these cases, the damping exhibits an intermediate \mathbf{q} -independent regime in between the quadratic and the linear wave-vector dependence. Specifically, we find

$$\Gamma_{\mathbf{q}} = \frac{N\hbar\beta^2 k_F}{8\pi\rho_0 a^2} \begin{cases} q^2 \ell / 2, & q \ll q_0 \\ q_0^2 \ell / 2, & q_0 \ll q \ll \frac{1}{\ell} \\ (c/v_F)^2 q, & q \gg \frac{1}{\ell} \end{cases} \quad (50)$$

for very weak intervalley scattering $q_0\ell_V \gg 1$ and

$$\Gamma_{\mathbf{q}} = \frac{N\hbar\beta^2 k_F}{8\pi\rho_0 a^2} \begin{cases} q^2 \ell / 2, & q \ll \frac{1}{\ell_V} \\ \ell / 2 \ell_V^2, & \frac{1}{\ell_V} \ll q \ll \frac{1}{(q_0\ell_V)^2 \ell} \\ (c/v_F)^2 q, & q \gg \frac{1}{(q_0\ell_V)^2 \ell} \end{cases} \quad (51)$$

for stronger intervalley scattering $q_0\ell_V \ll 1$.

Our results for the acoustic (in-plane) phonons of graphene are summarized in Figs. 3 and 4. For transverse synthetic fields, the damping rate crosses over from a quadratic to a linear dependence on q when $q \sim 1/\ell$. In contrast, when the damping is dominated by longitudinal fields, there

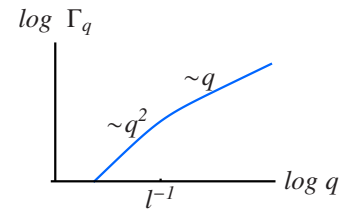


FIG. 4. (Color online) Schematic dependence of the damping rate $\Gamma_{\mathbf{q}}$ on wave-vector q for acoustic phonons in graphene when the transverse synthetic electric field is dominant, cf. Eq. (49). This applies for all directions of \mathbf{q} , except when the wave vector points in a narrow cone around the zigzag (armchair) direction for the longitudinal (transverse) acoustic phonon.

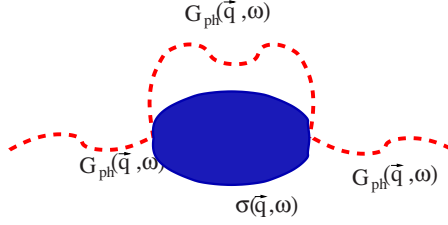


FIG. 5. (Color online) Sketch of the Feynman diagram for the damping rate of flexural phonons.

is an intermediate constant regime for $\max\{q_0, 1/\ell_V\} \ll q \ll \max\{1, 1/(q_0\ell_V)^2\}(1/\ell)$. In magnitude, the damping rate is the same for longitudinal and transverse electric fields for small q where we find a quadratic dependence on q in both cases. For larger q , the damping is much stronger for transverse fields. Deep in the ballistic regime $q\ell \gg 1$, where one finds a linear dependence on q in both cases, the ratio saturates at approximately $(v_F/c)^2 \approx 10^4$.

2. Flexural modes

We now turn to flexural modes of suspended graphene samples which are characterized by out-of-plane fluctuations $h(\mathbf{r}, t)$. A qualitative difference arises since, by symmetry, $h(\mathbf{r}, t)$ appears quadratically in the strain tensor. As a result, the coupling between electrons and flexural modes is quadratic rather than linear. This implies that the dominant damping mechanism involves both the creation of a particle-hole pair and a lower-energy flexural phonon.

The corresponding rate can be obtained from Fermi's golden rule (or alternatively, the Feynman diagram in Fig. 5). Quantizing the out-of-plane displacements (Figs. 6), we find at zero-temperature

$$\Gamma_{\mathbf{q}} = \frac{2\pi}{\hbar} \frac{1}{\Omega^4} \sum_{\epsilon_\beta > E_F} \sum_{\alpha < E_F} \sum_{\mathbf{q}'} |\langle \beta | v_F \sigma \cdot A_{\mathbf{q}-\mathbf{q}'} e^{i(\mathbf{q}-\mathbf{q}') \cdot \mathbf{r}} | \alpha \rangle|^2 \times \delta(\epsilon_\beta - \epsilon_\alpha - \omega_{\mathbf{q}} + \omega_{\mathbf{q}'}) \quad (52)$$

in terms of

$$A_{\mathbf{q}_1, \mathbf{q}_2} = \frac{\hbar\beta}{4a} \begin{pmatrix} q_{1x}q_{2y} + q_{1y}q_{2x} \\ q_{1x}q_{2x} - q_{1y}q_{2y} \end{pmatrix} \sqrt{\frac{\hbar\Omega}{2\rho_0\omega_{\mathbf{q}_1}}} \sqrt{\frac{\hbar\Omega}{2\rho_0\omega_{\mathbf{q}_2}}} \quad (53)$$

Following the approach of this paper, we rewrite this expression in terms of the dissipative conductivity Eq. (13),

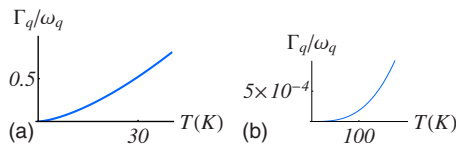


FIG. 6. (Color online) Inverse quality factor as function of temperature for long-wavelength flexural vibrations in graphene. The wave vector is $|\mathbf{q}|^{-1} = 1 \mu\text{m}$, the mean-free path is $l = 100 \text{ nm}$, and the carrier density is 10^{12} cm^{-2} . Left: no external tension. Right: external tension $\gamma = 0.02$.

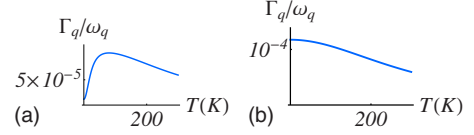


FIG. 7. (Color online) Temperature dependence of the inverse quality factor $\Gamma_{\mathbf{q}}/\omega_{\mathbf{q}}$ for acoustic phonons in graphene, induced by valley Coulomb drag, when damping is dominated by longitudinal (left) and transverse (right) synthetic electric field. Calculations have been done for an elastic mean-free path $\ell = 100 \text{ nm}$, $\tau_V = 200\tau$, $|\mathbf{q}| = (1 \mu\text{m})^{-1}$, and a carrier density $n = 10^{12} \text{ cm}^{-2}$. Note the enhancement of $\Gamma_{\mathbf{q}}$ for transverse synthetic fields.

$$\Gamma_{\mathbf{q}} = \frac{1}{2e^2\hbar\Omega} \left(\frac{\hbar\beta}{2a} \right)^2 \left(\frac{\hbar}{2\rho_0} \right)^2 \sum_{\mathbf{q}'} \frac{\omega_{\mathbf{q}} - \omega_{\mathbf{q}'}}{\omega_{\mathbf{q}}\omega_{\mathbf{q}'}} \times \sigma_{s,ij}(\mathbf{q} - \mathbf{q}', \omega_{\mathbf{q}} - \omega_{\mathbf{q}'}) \times \begin{pmatrix} q_x q'_y + q_y q'_x \\ q_x q'_x - q_y q'_y \end{pmatrix}_i \begin{pmatrix} q_x q'_y + q_y q'_x \\ q_x q'_x - q_y q'_y \end{pmatrix}_j \quad (54)$$

As we have seen above, the conductivity tensor is dominated by the transverse conductivity so that

$$\sigma_{s,ij}(\mathbf{q}, \omega) \approx \sigma_{\perp}(\mathbf{q}, \omega) \left(\delta_{ij} - \frac{q_i q_j}{q^2} \right). \quad (55)$$

At finite temperature $T \gg \omega_{\mathbf{q}}$, the integrand in Eq. (54) is modified to include an extra factor $T/\hbar\omega_{\mathbf{q}'}$ which is a consequence of the existence of a phonon in the final state.

We first focus on ideal graphene membranes for which the dispersion of flexural phonons is quadratic, $\omega_{\mathbf{q}} = \alpha q^2$ (where $\alpha = \sqrt{\kappa/\rho_0}$). In this case, we find for the angular average of the damping rate

$$\Gamma_{\mathbf{q}} \sim \begin{cases} \frac{N\hbar^2\beta^2 k_F \ell}{\rho_0^2 a^2 \alpha} q^4, & q\ell \ll 1 \\ \frac{N\hbar^2\beta^2 k_F}{\rho_0^2 a^2 \alpha} q^3, & q\ell \gg 1 \end{cases} \quad (56)$$

in the low-temperature limit $T \ll \hbar\alpha q^2$ and

$$\Gamma_{\mathbf{q}} \sim \begin{cases} \frac{N\hbar^2\beta^2 k_F \ell}{\rho_0^2 a^2 \alpha} \left(\frac{T}{\hbar\alpha} \right)^2, & T \ll \hbar\alpha/\ell^2 \\ \frac{N\hbar^2\beta^2 k_F}{\rho_0^2 a^2 \alpha} \left(\frac{T}{\hbar\alpha} \right)^{3/2}, & T \gg \hbar\alpha/\ell^2 \end{cases} \quad (57)$$

in the high-temperature regime $T \gg \hbar\alpha q^2$. Because of the low frequency of pure flexural phonons, the vibrations can become overdamped at finite temperature.

If the graphene membrane is under tension γ [inducing a term $\sim (\nabla h)^2$ in the elastic Lagrangian], the dispersion of the flexural phonons becomes linear at long wavelengths, $\omega_{\mathbf{q}} = c_f q$. In this case, we find for the angular average of the damping rate

$$\Gamma_{\mathbf{q}} \sim \begin{cases} \frac{N\hbar^2\beta^2k_F\ell}{\rho_0^2a^2c_f}q^5, & q\ell \ll 1 \\ \frac{N\hbar^2\beta^2k_F}{\rho_0^2a^2c_f}q^4, & q\ell \gg 1 \end{cases} \quad (58)$$

in the low-temperature regime $T \ll \hbar c_f q$ and

$$\Gamma_{\mathbf{q}} \sim \begin{cases} \frac{N\hbar^2\beta^2k_Fq\ell}{\rho_0^2a^2c_f} \left(\frac{T}{\hbar c_f}\right)^4, & T \ll \hbar c_f/\ell \\ \frac{N\hbar^2\beta^2k_Fq}{\rho_0^2a^2c_f} \left(\frac{T}{\hbar c_f}\right)^3, & T \gg \hbar c_f/\ell \end{cases} \quad (59)$$

in the high-temperature $T \gg \hbar c_f q$ regime.³⁴

Actual suspended samples are typically expected to be under some degree of tension. The magnitude of phonon damping will then depend critically on the sample-specific degree of tension, which enters through the mode velocity $c_f = c\sqrt{\gamma}$. It is interesting to point out that unlike in-plane modes, the damping of flexural modes is temperature dependent in the degenerate limit $E_F \gg T$, even in the absence of electron-electron interactions.

IV. COULOMB INTERACTION EFFECTS ON PHONON DAMPING

A. Damping by valley Coulomb drag in graphene

Electron-electron interactions lead to interesting temperature dependence of the phonon damping which persists even in clean samples. In fact, it is a well-known effect of spintronics that spin currents decay due to electron-electron interactions even in the absence of disorder since unlike charge currents, they are not protected by momentum conservation. By analogy, the valley currents driven by the electric fields associated with the vector potential will dissipate by intervalley Coulomb scattering. A theory of this effect must go beyond existing works on Coulomb drag in that one has to account for the *ac* nature of the driving valley-odd electric field.

This is easily accomplished in the diffusive limit where we can amend the hydrodynamic equations to include the intervalley electron-electron scattering. While the continuity equations remain unchanged, Ohm's laws take the form

$$\left(\frac{1}{\tau} + \frac{1}{\tau_V} + \frac{1}{\tau_D}\right)\mathbf{j}_1 - \left(\frac{1}{\tau_D} + \frac{1}{\tau_V}\right)\mathbf{j}_2 = -\frac{v_F^2}{2}\nabla\rho_1 + \frac{e^2v_F^2}{2}\mathbf{E}_1, \quad (60)$$

$$-\left(\frac{1}{\tau_D} + \frac{1}{\tau_V}\right)\mathbf{j}_1 + \left(\frac{1}{\tau} + \frac{1}{\tau_V} + \frac{1}{\tau_D}\right)\mathbf{j}_2 = -\frac{v_F^2}{2}\nabla\rho_2 + \frac{e^2v_F^2}{2}\mathbf{E}_2. \quad (61)$$

Here, $1/\tau_D \sim T^2/E_F$ (possibly up to logarithmic factors from $2k_F$ scattering) is the intervalley scattering rate responsible for the drag effect. (Coulomb drag in doped graphene is expected to have the same features as in other 2D electronic systems).³⁰ It is then evident that valley Coulomb drag can be accounted for by evaluating the dc conductivity σ_{dc} and

the diffusion constant D with the effective scattering rate

$$\frac{1}{\tau_{\text{eff}}} = \frac{1}{\tau} + \frac{2}{\tau_V} + \frac{2}{\tau_D}. \quad (62)$$

Thus, the dissipation is dominated by the drag effect (disorder scattering) when $T > T^*$ ($T < T^*$), where

$$T^* \sim \sqrt{\frac{E_F}{\tau}} \sim \frac{E_F}{\sqrt{k_F\ell}}. \quad (63)$$

Here, we used that for realistic samples, disorder predominantly causes intravalley scattering. For realistic parameters in suspended graphene, we estimate $T^* \approx 10\text{--}100$ K.

The inclusion of valley Coulomb drag allows us to discuss the temperature dependence of the intrinsic phonon damping in clean (but doped) graphene. The intervalley electron-electron scattering leads to a temperature-dependent mean-free path $\sim \hbar v_F E_F / T^2$. Thus, when holding the wavevector \mathbf{q} fixed, we find that the damping will follow the behavior of the ballistic (diffusive) regime for $T < T_{\mathbf{q}}^*$ ($T > T_{\mathbf{q}}^*$), where

$$T_{\mathbf{q}}^* \sim \sqrt{E_F(\hbar v_F q)}. \quad (64)$$

As a result, we find for fixed \mathbf{q} and when the damping is dominated by the transverse synthetic electric field that $\Gamma_{\mathbf{q}}$ is constant for temperatures smaller than $T_{\mathbf{q}}^*$ (determined by the transverse conductivity in the ballistic regime) and decreases monotonically as $\propto 1/T^2$ as the system enters the diffusive regime for $T > T_{\mathbf{q}}^*$. This remarkable temperature dependence is a consequence of the fact that the dissipation is proportional to the scattering time and thus inversely proportional to the scattering rate (see Fig. 7).

In the presence of disorder, the temperature dependence also crosses over from constant to monotonically decreasing as $\propto 1/T^2$. This crossover occurs at $T_{\mathbf{q}}^*$ when $q\ell \gg 1$ and at T^* when $q\ell \ll 1$. When the synthetic electric field is purely longitudinal, there can be an intermediate regime (for $T > T_{\mathbf{q}}^*$ in the clean limit) in which the damping rate increases as T^2 before it crosses over into the $\propto 1/T^2$ behavior beyond a temperature $(v_F/c)^{1/2}T_{\mathbf{q}}^*$.

B. Damping by valley Coulomb drag in carbon nanotubes

Valley Coulomb drag also affects the damping of phonon modes of carbon nanotubes. For the radial breathing mode of metallic carbon nanotubes, the effect may be significant since phonon damping is dominated by the decay of valley currents. Moreover, it is natural to expect that Coulomb drag is particularly effective in a one-dimensional setting. In contrast, we expect that valley Coulomb drag is less significant for the longitudinal stretching mode where damping is dominated by the effects of the scalar potential. In this case, damping by decay of valley currents is only a subleading contribution. Nevertheless, it is worthwhile to remark that valley Coulomb drag provides the dominant damping mechanism based on the electron-phonon interaction in the strictly clean limit.

A detailed theory of valley Coulomb drag in carbon nanotubes must account for possible electronic correlation effects

associated with the Luttinger liquid nature of the electron system. Such a theory is beyond the scope of the present paper.

V. CONCLUSIONS

We have considered the damping of low-energy phonons in carbon nanotubes and graphene originating from the electron-phonon interaction. For most phonon modes, this damping is closely related to a synthetic electric field associated with a strain-induced vector potential in the Dirac equation for the electronic properties of graphene. We find that it is very instructive to analyze phonon damping in terms of these synthetic electric fields: (i) within this approach, phonon damping is a direct consequence of Joule heating. (ii) This establishes a close relation between phonon damping and the dynamic conductivity which we exploit to derive damping rates in the presence of disorder and electron-electron interactions. (iii) We find rich physics emerging from the fact that the synthetic electric field has opposite signs in the two valleys. Most prominently, we identify valley Coulomb drag as an important dissipation channel which leads to unconventional temperature dependence of the damping rate.

Throughout this paper, we have considered idealized samples in the sense that we ignored finite-size effects and electrodes. Clearly, when suspended carbon nanotubes or graphene membranes are coupled to electrodes, there will be (additional) electronic dissipation taking place in the leads even if the nanotube is otherwise perfectly ballistic. While the physics of this damping is certainly highly nonuniversal, a rough estimate may be obtained from our expressions for diffusive electronic dynamics by setting the elastic mean-free path equal to the length of the carbon nanotube or the linear dimension of the graphene membrane. It is also worthwhile to point out that the electron-phonon coupling is not expected to change significantly in multilayer graphene samples. Thus, our results should also be applicable in these systems.

Our results should be of direct relevance to the intense ongoing experimental efforts to build and explore nanomechanical as well as nanoelectromechanical devices based on graphene nanostructures. We expect the electron-phonon interaction to be the dominant source of phonon damping whenever the system exhibits a metallic conductivity. In such systems, our results should be valuable by providing upper bounds on the quality factor as well as by guiding optimization strategies.

ACKNOWLEDGMENTS

We would like to thank M. Polini for helpful discussions, and Y. Galperin for drawing our attention to the importance of intervalley scattering. This work was supported in part by the Deutsche Forschungsgemeinschaft through Grants No. Sfb 658 and No. SPP 1243, and DIP (F.v.O.) by MEC (Spain) through Grant No. FIS2008-00124 and CONSOLIDER through Grant No. CSD2007-00010, and by the Comunidad de Madrid, through CITECNOMIK (FG). F.v.O.

and P.G. acknowledge the hospitality of the KITP at UCSB, where research was supported in part by the National Science Foundation under Grant No. PHY05-51164.

APPENDIX: DYNAMIC CONDUCTIVITY OF GRAPHENE IN THE BALLISTIC REGIME

Here, we sketch the derivation of the longitudinal conductivity in the ballistic regime, including the effect of intervalley disorder scattering. We start from Boltzmann equations with valley electric field \mathbf{E} for the two valleys,

$$\begin{aligned} & \left(-i\omega + i\mathbf{v}_{\mathbf{p}} \cdot \mathbf{q} + \frac{e\mathbf{E}}{2} \cdot \nabla_{\mathbf{p}} \right) n_{\mathbf{p}}^{(1)} \\ &= \frac{1}{\Omega\nu\tau_V} \sum_{\mathbf{p}'} \delta(\epsilon_{\mathbf{p}} - \epsilon_{\mathbf{p}'}) (n_{\mathbf{p}'}^{(2)} - n_{\mathbf{p}}^{(1)}), \end{aligned} \quad (\text{A1})$$

$$\begin{aligned} & \left(-i\omega + i\mathbf{v}_{\mathbf{p}} \cdot \mathbf{q} - \frac{e\mathbf{E}}{2} \cdot \nabla_{\mathbf{p}} \right) n_{\mathbf{p}}^{(2)} \\ &= \frac{1}{\Omega\nu\tau_V} \sum_{\mathbf{p}'} \delta(\epsilon_{\mathbf{p}} - \epsilon_{\mathbf{p}'}) (n_{\mathbf{p}'}^{(1)} - n_{\mathbf{p}}^{(2)}), \end{aligned} \quad (\text{A2})$$

where $n_{\mathbf{p}}^{(j)}$ denotes the distribution function in valley j . Here we include the intervalley disorder scattering which is required to obtain results which match the diffusive results. Taking the difference between these two equations, we obtain an equation for the odd distribution function $\Delta n_{\mathbf{p}} = n_{\mathbf{p}}^{(1)} - n_{\mathbf{p}}^{(2)}$,

$$\begin{aligned} & \left(-i\omega + i\mathbf{v}_{\mathbf{p}} \cdot \mathbf{q} + \frac{1}{\tau_V} \right) \Delta n_{\mathbf{p}} + e\mathbf{E} \cdot \nabla_{\mathbf{p}} n_{\mathbf{p}}^{(\text{eq})} \\ &= -\frac{1}{\Omega\nu\tau_V} \sum_{\mathbf{p}'} \delta(\epsilon_{\mathbf{p}} - \epsilon_{\mathbf{p}'}) \Delta n_{\mathbf{p}'}. \end{aligned} \quad (\text{A3})$$

Here, we assumed linear response and $n_{\mathbf{p}}^{(\text{eq})}$ denotes the Fermi-Dirac distribution. Introducing the Fermi surface deformation $\delta\nu(\phi)$ by $\Delta n_{\mathbf{p}} = \delta(\epsilon_{\mathbf{p}} - \mu) \delta\nu(\phi)$ and introducing the angle $\phi = \angle(\mathbf{q}, \mathbf{p}) = \angle(\mathbf{E}, \mathbf{p})$, we find

$$\delta\nu(\phi) = \frac{eE v_F \cos \phi - \frac{1}{\tau_V} \langle \delta\nu(\phi) \rangle}{-i\omega + i v_F q \cos \phi + \frac{1}{\tau_V}}. \quad (\text{A4})$$

In the absence of interlayer scattering, we find for the density $\rho = e\nu \int (d\phi/2\pi) \delta\nu(\phi)$ the conventional result

$$\rho = \frac{e^2 \nu}{iq} E. \quad (\text{A5})$$

From the expression for the current, $j = e\nu v_F \int (d\phi/2\pi) \cos \phi \delta\nu(\phi)$, we obtain the (dissipative) longitudinal conductivity

$$\sigma_{\parallel}(\mathbf{q}, \omega) = \frac{e^2 \nu \omega^2}{v_F q^3}. \quad (\text{A6})$$

Equation (A4) shows that in the presence of intervalley scattering, there is an additional contribution (proportional to

$1/\tau_V$) to the current. In this term, we can evaluate $\langle \delta v(\phi) \rangle$ using the result for $\delta v(\phi) \simeq eE/iq$ in the absence of intervalley scattering. Noting that we may also replace $\cos \phi$ in the first term by $\omega/v_F q$, we find that the second term dominates

as long as $q \ll [(q_0 \ell_V) \ell]^{-1}$ while the first term dominates for $q \gg [(q_0 \ell_V) \ell]^{-1}$. Evaluating the longitudinal conductivity then gives the results quoted in Eq. (47).

-
- ¹K. S. Novoselov, A. K. Geim, S. V. Morozov, D. Jiang, Y. Zhang, S. V. Dubonos, I. V. Grigorieva, and A. A. Firsov, *Science* **306**, 666 (2004).
- ²K. S. Novoselov, D. Jiang, F. Schedin, T. J. Booth, V. V. Khotkevich, S. V. Morozov, and A. K. Geim, *Proc. Natl. Acad. Sci. U.S.A.* **102**, 10451 (2005).
- ³A. H. Castro Neto, F. Guinea, N. M. R. Peres, K. S. Novoselov, and A. K. Geim, *Rev. Mod. Phys.* **81**, 109 (2009).
- ⁴J. González, F. Guinea, and M. A. H. Vozmediano, *Phys. Rev. Lett.* **69**, 172 (1992).
- ⁵H. Suzuura and T. Ando, *Phys. Rev. B* **65**, 235412 (2002).
- ⁶S. V. Morozov, K. S. Novoselov, M. I. Katsnelson, F. Schedin, L. A. Ponomarenko, D. Jiang, and A. K. Geim, *Phys. Rev. Lett.* **97**, 016801 (2006).
- ⁷J. L. Mañes, *Phys. Rev. B* **76**, 045430 (2007).
- ⁸A. F. Morpurgo and F. Guinea, *Phys. Rev. Lett.* **97**, 196804 (2006).
- ⁹F. Guinea, M. I. Katsnelson, and M. A. H. Vozmediano, *Phys. Rev. B* **77**, 075422 (2008).
- ¹⁰E. Mariani and F. von Oppen, *Phys. Rev. Lett.* **100**, 076801 (2008).
- ¹¹F. Guinea, B. Horowitz, and P. Le Doussal, *Phys. Rev. B* **77**, 205421 (2008).
- ¹²K.-i. Sasaki, R. Saito, G. Dresselhaus, M. S. Dresselhaus, H. Farhat, and J. Kong, *Phys. Rev. B* **78**, 235405 (2008).
- ¹³A. De Martino, R. Egger, and A. Gogolin, *Phys. Rev. B* **79**, 205408 (2009).
- ¹⁴I. D'Amico and G. Vignale, *EPL* **55**, 566 (2001).
- ¹⁵K. Flensberg, T. S. Jensen, and N. A. Mortensen, *Phys. Rev. B* **64**, 245308 (2001).
- ¹⁶C. P. Weber, N. Gedik, J. E. Moore, J. Orenstein, J. Stephens, and D. D. Awschalom, *Nature (London)* **437**, 1330 (2005).
- ¹⁷B. J. LeRoy, S. G. Lemay, J. Kong, and C. Dekker, *Nature (London)* **432**, 371 (2004).
- ¹⁸R. Rao, J. Menendez, C. D. Poveleit, and A. M. Rao, *Phys. Rev. Lett.* **99**, 047403 (2007).
- ¹⁹S. Sapmaz, P. Jarillo-Herrero, Y. M. Blanter, C. Dekker, and H. S. J. van der Zant, *Phys. Rev. Lett.* **96**, 026801 (2006).
- ²⁰B. Witkamp, M. Poot, and H. S. J. van der Zant, *Nano Lett.* **6**, 2904 (2006).
- ²¹A. K. Hüttel, M. Poot, B. Witkamp, and H. S. J. van der Zant, *New J. Phys.* **10**, 095003 (2008).
- ²²R. Leturcq, C. Stampfer, K. Inderbitzin, L. Durrer, C. Hierold, E. Mariani, M. G. Schultz, F. von Oppen, and K. Ensslin, *Nat. Phys.* **5**, 327 (2009).
- ²³D. Garcia-Sanchez, A. San Paulo, M. J. Esplandiu, F. Perez-Murano, L. Forró, A. Aguasca, and A. Bachtold, *Phys. Rev. Lett.* **99**, 085501 (2007).
- ²⁴J. S. Bunch, A. M. van der Zande, S. S. Verbridge, I. W. Frank, D. M. Tanenbaum, J. M. Parpia, H. G. Craighead, and P. L. McEuen, *Science* **315**, 490 (2007).
- ²⁵D. Garcia-Sanchez, A. M. van der Zande, A. S. Paulo, B. Lassagne, P. L. McEuen, and A. Bachtold, *Nano Lett.* **8**, 1399 (2008).
- ²⁶J. Koch and F. von Oppen, *Phys. Rev. Lett.* **94**, 206804 (2005).
- ²⁷J. Koch, F. von Oppen, and A. V. Andreev, *Phys. Rev. B* **74**, 205438 (2006).
- ²⁸M. Pomerantz, R. W. Keyes, and P. Seiden, *Phys. Rev. Lett.* **9**, 312 (1962).
- ²⁹B. I. Halperin, P. A. Lee, and N. Read, *Phys. Rev. B* **47**, 7312 (1993).
- ³⁰W.-K. Tse, Ben Yu-Kuang Hu, and S. Das Sarma, *Phys. Rev. B* **76**, 081401(R) (2007).
- ³¹Formally, this can be achieved by employing a gauge transformation at the beginning of the calculation which eliminates the scalar potential at the expense of introducing an additional contribution to the vector potential. Undoing the gauge transformation at the end of the calculation shows that the scalar potential enters as shown in Eq. (14).
- ³²We note that the description of the synthetic fields as electric and magnetic fields is motivated by their effect on the Dirac carriers. At the same time, the dynamics of these fields is entirely controlled by elasticity theory which has little resemblance to electrodynamics.
- ³³The crossover occurs at $q \sim 1/\ell$ when $q_0 \ell_V \gg 1$ and at $q \sim 1/\ell_V$ when $q_0 \ell \ll 1$. A more accurate expression for the function $f(\theta)$ can be readily derived by including both the longitudinal and the transverse components of the synthetic electric field in the calculation of the damping rate.
- ³⁴In principle, there are also intermediate cases in which the dispersion is linear at long wavelengths due to tension but becomes quadratic at larger q . Our results can be extended to this situation but we refrain from giving explicit results.